Shape of impact craters in granular media

Simon J. de Vet* and John R. de Bruyn†
Department of Physics and Astronomy, University of Western Ontario, London, Ontario, Canada N6A 3K7
(Received 15 August 2007; published 30 October 2007)

We present the results of experiments studying the shape of craters formed by the normal impact of a solid spherical projectile into a deep noncohesive granular bed at low energies. The resultant impact crater surfaces are accurately digitized using laser profilometry, allowing for the detailed investigation of the crater shape. We find that these impact craters are very nearly hyperbolic in profile. Crater radii and depths are dependent on impact energy, as well as the projectile density and size. The precise crater shape is a function of the crater aspect ratio. While the dimensions of the crater are highly dependent on the impact energy, we show that the energy required to excavate the crater is only a tiny fraction (0.1%–0.5%) of the kinetic energy of the projectile.

DOI: 10.1103/PhysRevE.76.041306 PACS number(s): 45.70.−n, 83.80.Fg, 96.15.Qr

I. INTRODUCTION

Impact craters are ubiquitous on rocky bodies throughout the solar system, and in many cases are the dominant surface landforms. The process of crater formation is complex. It is difficult to observe cratering directly, and much of our understanding of the process derives from observations of the end product, that is, the craters themselves. Crater formation has also been studied by firing very high speed projectiles at solid targets [1], and sophisticated computer models have been developed, which incorporate much of the detailed physics [2,3].

Impacts into granular materials were investigated to some extent decades ago [4]. Recently there has been substantial interest in the study of impacts into granular materials [5–15], stemming largely from an interest in granular flows in general [16], and, in particular, from a desire to understand the drag force on an object moving through granular materials and the effective rheology of granular materials under a variety of conditions [10–15]. The scaling of crater dimensions with impact energy and other parameters has been studied [6,9,12] as has the penetration of the projectile into the granular medium [5,10,14]. Experiments on granular impacts may also be relevant to planetary impact processes, even though their energies are typically many orders of magnitude smaller than those of meteor impacts. For example, experiments by Walsh *et al.* [6] on impacts into a container of glass beads showed a progression of crater morphologies as a function of impact energy that mirrored that seen in lunar craters [17].

Here we describe measurements of the *shapes* of craters formed by low-energy impacts in granular materials. At the lowest energies, so-called simple craters form, characterized by a bowl-like profile and a distinct raised rim [6]. At somewhat higher energies, a granular jet forms as the cavity formed by the penetration of the sphere into the granular target collapses [18,19]. This leads to the formation of a peak in the center of the crater [6]. Similar morphologies are observed in planetary craters [17]. Our craters were formed by the impact of spherical projectiles falling vertically into a target consisting of small noncohesive spherical glass beads. The crater surfaces were digitized in three dimensions using a scanning laser profilometer. Azimuthally averaged crater profiles were used to determine crater dimensions and to study the crater shape over several orders of magnitude in impact energy. We find that, away from the rim, the impact craters are nearly hyperbolic in profile with a remarkably consistent maximum slope. The measured crater profiles are also used to investigate the energetics of the crater formation process, giving the rather surprising result that the energy required to excavate the crater is only a very small fraction of the energy delivered by the projectile.

II. EXPERIMENT

The experiments were performed by releasing spherical projectiles from a holder so that they fell vertically and without rotation into a container of small spherical glass beads. Three sizes of glass beads were used as target materials [20]: one with diameters in the range of 200–425 μm, one with diameters of 180–300 μm, and one with diameters of 106–212 μm. The beads were used as provided by the manufacturer. In our experiments, we found crater size and shape to be independent of the bead size used.

The granular target is prepared by pouring the granular particles from a height of roughly 20 cm, without shaking or stirring, into a cylindrical metal container 19 cm in depth and 24 cm in diameter. The container is overfilled, and the surface leveled using a straightedge. This method generates a loose close packed granular target with a packing fraction of 0.60 ± 0.01. Packing fractions were determined from measurements of the mass and volume of the bulk granular material, taking the glass density to be $\rho_b = 2500\ \mathrm{kg/m^3}$. The initial conditions are reproducible on the bulk scale, although differences in bead packing at the small scale are unavoidable and have a small effect on the resultant craters.

Ten different spheres were used as projectiles, having radii r_p ranging from 0.4 to 2.0 cm and densities ρ_p ranging from 2500 (glass) to 15 000 $\mathrm{kg/m^3}$ (tungsten carbide). The properties of the projectiles are summarized in Table I. The

*sdevet@uwo.ca
†debruyn@uwo.ca

TABLE I. Properties of the projectiles used to create impact craters.

Material	Radius r_p (mm)	Density ρ_p (kg/m^3)
Glass	3.95	2688
Glass	4.88	2919
Glass	8.10	2493
Glass	12.50	2473
Steel	3.97	7801
Steel	6.34	7803
Steel	12.69	7907
Steel	19.06	7776
Lead	19.26	10090
Tungsten carbide	6.35	15010

surface roughness for these projectiles has been measured, and is on the order of 0.1–1 μm in amplitude. The amplitude of the surface roughness does not correlate in any way to the size or shape of the resultant craters.

To produce a crater, a projectile is dropped from a height h above the center of the granular target. A fresh granular target is prepared for each experiment. Only craters for which the projectile was completely buried in the target material were studied. This constraint determines the minimum drop height, which was about 3 cm for the higher-density metal projectiles and 35 cm for the low-density glass projectiles. The velocity v of the projectile at impact is given by $v=\sqrt{2gh}$, where g is the acceleration due to gravity, and ranges from 0.6 to 4.4 m/s. The kinetic energy of the projectile at impact, given by $E=\frac{4}{3}\pi r_p^3 \rho_p g h$, is in the range 6×10^{-4} J$\leq E\leq$0.66 J.

The surface of each crater is accurately digitized in three dimensions using a home-built laser profilometer, illustrated schematically in Fig. 1. A low power HeNe laser beam with a wavelength of 633 nm passes through a cylindrical lens and expands into a fan-shaped laser sheet. The laser sheet strikes an angled mirror, which directs it towards the granular surface, which it strikes at an oblique angle, fixed arbitrarily at θ=42.3°. If the granular surface were flat then the laser sheet would appear as a straight line on the surface. We define this line to be parallel to the y direction. If the surface is not flat, the laser line will be curved when viewed from above. If a point on the line is detected at position coordinates (x,y), and the undeviated (flat surface) line would have been at (x_l,y), then the vertical (z) coordinate of the surface is given by

$$z=(x-x_l)\tan\theta, \tag{1}$$

where we have defined the original flat surface to be at $z=0$. Thus the interior of the crater has $z<0$ and the raised crater rim has $z>0$. The laser line extends well to either side of the crater in the y direction, so the undeviated line position x_l is found from the undisturbed bed surface far from the crater.

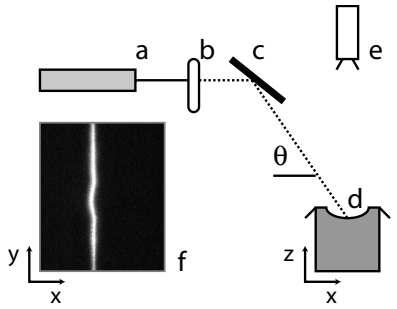

FIG. 1. A schematic view of the laser profilometer. A laser beam (a) passes through a cylindrical lens (b) spreading it into a fan-shaped laser sheet (dotted line). An angled mirror (c) directs the laser sheet onto the crater surface (d) at an oblique angle θ. A CCD camera (e) mounted above the crater surface captures an image (f), which is digitally processed to determine the laser line position. The mirror is translated horizontally to scan the laser line across the entire crater surface. The local deviation of the detected laser line from a straight line is proportional to the local depth of the crater surface.

A computer-controlled stepper motor translates the angled mirror, sweeping the laser line across the entire crater surface. A CCD camera interfaced to the computer is used to record images of the laser line from above at a sampling frequency of one image every 0.5 mm, corresponding to several hundred lines across the diameter of a typical crater. The line position x is determined at each y coordinate from an intensity-weighted average across the line. The resolution of y is determined by the camera resolution, and is measured every 0.2 mm. Processing all lines from a scan results in a full three-dimensional representation of the crater surface with an accuracy in z of ±0.25 mm. A typical digitized crater surface is shown in Fig. 2.

To investigate the crater shape quantitatively or to determine crater dimensions it is convenient to assume rotational symmetry. The crater shown in Fig. 2 is almost perfectly rotationally symmetric in the interior, but the rim is slightly irregular and the small central peak is slightly off center. We convert the raw three-dimensional data into a two-dimensional (height z vs radial distance r) profile by locating the center of the crater numerically, binning the data in radial bins of width 0.5 mm, and averaging. An example of a two-dimensional crater profile obtained in this way is illustrated in Fig. 3.

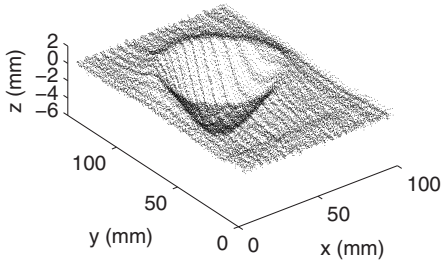

FIG. 2. A typical digitized crater surface, in this case for a steel projectile of r_p=13 mm dropped from a height of 1 m into the largest size of glass beads. To emphasize crater shape, the z axis has been exaggerated by 5× relative to the x and y axes. For clarity, only every fifth point is plotted.

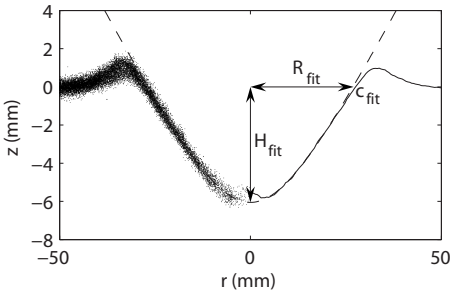

FIG. 3. A typical averaged crater profile with a small central peak, in this case generated from the raw data shown in Fig. 2. The left-hand side of the figure shows the raw data points, while the solid line on the right is the azimuthally averaged profile. The dashed line is the hyperbolic profile fit to the data. R_{fit} is the radius of the hyperbola at $z=0$, H_{fit} is the depth of the hyperbola at $r=0$, and c_{fit} is the slope of the profile at $r=R_{fit}$ and $z=0$. As in Fig. 2, the vertical axis has been exaggerated by 5× for clarity, and only one in five of the raw data points is plotted.

III. RESULTS

At the lowest impact energies we find simple craters with no central peak. Simple craters have been referred to as "bowl shape," or "nearly parabolic" in the literature [17,21]. We attempted to fit the interior portion of our measured crater profiles, away from the crater rim, with various functional forms. For consistency we fit that part of the profile falling between the lowest point in the crater, which is usually a few mm out from $r=0$ due to the presence of a central peak, and a line 3/4 of the way to the $z=0$ surface. We find that all of our profiles (including those with a central peak), over several orders of magnitude in impact energy, are well described by a hyperbola in the form

$$z = z_c + \sqrt{b^2 + c^2 r^2}, \tag{2}$$

where z_c, b, and c are fitting parameters. Fits to a parabolic function are less good, giving a χ^2 goodness-of-fit statistic that is roughly five times larger than the hyperbolic fits. The dashed line in Fig. 3 is the hyperbolic fit to the profile shown there. This fit describes the data extremely well over the domain of the fit, but, as expected, starts to diverge from the data closer to the crater rim and in the region of the central peak, both of which are outside of the fitting domain.

For further analysis, it is convenient to reparametrize our hyperbolic fits in terms of more physically meaningful quantities. The depth of the hyperbola at $r=0$ is given by $H_{fit}=-(z_c+b)$, and the radius of the hyperbola at $z=0$ is given as $R_{fit}=\sqrt{z_c^2-b^2}/c$. These two dimensions define the size and aspect ratio of the crater, but are not sufficient to fully characterize the crater shape. As a third parameter, we use the slope of the hyperbola at $z=0$, $c_{fit}=c\sqrt{1-b^2/z_c^2}$. These quantities are also illustrated in Fig. 3.

Figure 4(a) shows H_{fit}, the depth of the craters as determined from the hyperbolic fits, plotted as a function of the kinetic energy E of the projectile at impact. As expected [6], the crater depth increases with increasing E, but the impact energy is not the only relevant parameter in determining the crater depth. As Fig. 4(a) shows, for impacts of equal energy,

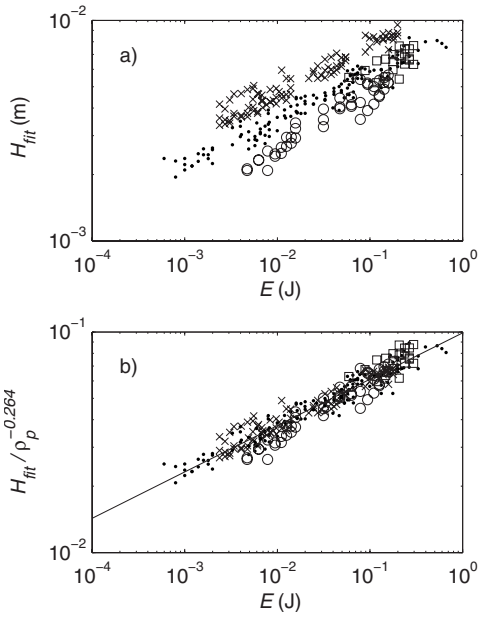

FIG. 4. Hyperbolic depth H_{fit} as a function of both impact energy E and projectile density ρ_p. In order of increasing density (see Table I), × are glass projectiles, ● are steel, □ are lead, and ○ are tungsten carbide. In (a), H_{fit} is plotted against impact energy E. In (b), the dependence on projectile density has been scaled out. The solid line is a least-squares power-law fit.

the lowest-density projectiles (glass) produce deeper craters than the higher-density projectiles (tungsten carbide). A least-squares fit to a power law in energy and density yields $H_{fit}=(0.099\pm0.008)E^{0.210\pm0.004}\rho_p^{-0.264\pm0.008}$. Uncertainties for this, and for all fits discussed below, were estimated using Monte Carlo methods [22]. This parameter dependence is illustrated in Fig. 4(b). H_{fit} shows no further dependence on projectile radius.

We find that the hyperbolic fit radius R_{fit}, on the other hand, depends on the impact energy E and on the projectile radius r_p, with no measurable density dependence. As above, we fit the data to a power law in both E and r_p to find $R_{fit}=(0.15\pm0.01)E^{0.226\pm0.005}r_p^{0.22\pm0.02}$. This form provides a good fit to the data for all but the largest projectiles, for which the R_{fit}, but not H_{fit}, is anomalously large. This is illustrated in Fig. 5. Scaling relations determined for several important crater dimensions are summarized in Table II.

The slope parameter c_{fit} obtained from the hyperbolic fits characterizes the shape of the crater. We find that it is not a simple function of the impact parameters, but is best described in terms of the crater aspect ratio R_{fit}/H_{fit}. The aspect ratio itself is dependent on both the projectile density and size, but is almost completely independent of the impact energy. c_{fit} is plotted as a function of the aspect ratio in Fig. 6. A perfectly conical crater would have $c_{fit}=(R_{fit}/H_{fit})^{-1}$, as indicated by the dashed line in Fig. 6, while rounder craters will have larger values of c_{fit}. We find that for the smallest aspect ratios (smaller, lower-density projectiles) c_{fit} is close to the conical limit, while at large aspect ratios ($R_{fit}/H_{fit} \gtrsim 4$) $c_{fit} \approx 0.33$, or close to 18°, independent of aspect ratio. For our granular materials, the angle of repose (the maximum stable angle of a free granular surface) is about 28°,

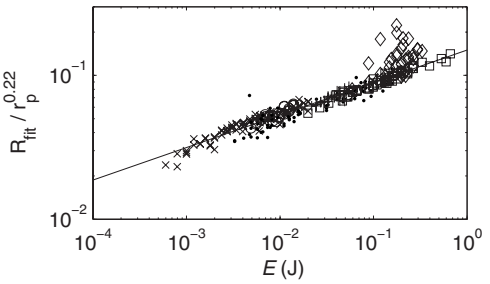

FIG. 5. Hyperbolic radius R_{fit} as a function of both impact energy and projectile radius. Here, a scaled radius $R_{fit}/r_p^{0.22}$ is plotted against impact energy. The solid line is the least-squares fit. In this plot, × are 4 mm radius projectiles, ○ are 5 mm, ● are 6 mm, + are 8 mm, □ are 13 mm, and ◇ are 19 mm. This scaling describes the behavior of all but the largest projectiles, which produce anomalously large craters.

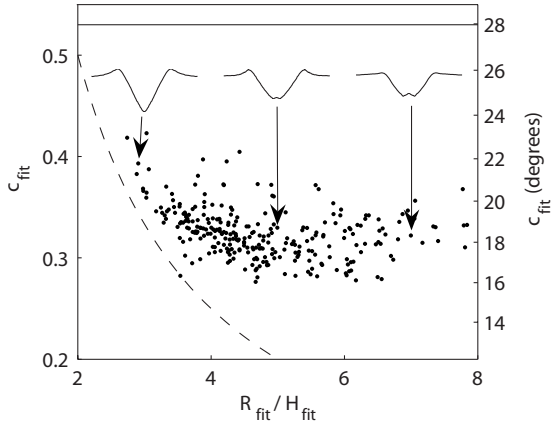

FIG. 6. Slope at $z=0$, c_{fit} as a function of the crater aspect ratio, R_{fit}/H_{fit}. At small aspect ratios, the slope is close to that expected from a conical crater (dashed line). At large aspect ratios, the slope approaches a constant value of about 0.33. All slopes are less than the repose slope for the granular materials (solid line at slope 0.53, or 28°). Also illustrated are sample profiles for aspect ratios of 3, 5, and 7. At the smallest aspect ratio, the crater slope is relatively large and the crater profile is nearly conical. As the crater aspect ratio increases, the slope approaches a constant value around 18°. These profiles have been scaled to the same radius. In each case, there is a 5× vertical exaggeration for clarity.

corresponding to a slope of 0.53. All of the measured crater slopes are significantly below this value. Similar results are obtained from analysis of either the actual profile slope at $z=0$ or the maximum slope of the full profile, which usually occurs very near $z=0$.

In addition to measuring crater dimensions associated with a hyperbolic fit, we can measure actual crater dimensions accurately and consistently. In what follows we use the azimuthally averaged profiles. We define the true crater depth H as the distance between the lowest point in the crater and the unperturbed $z=0$ surface. H and H_{fit} are generally quite close, with the real crater being slightly shallower than the fit in cases where there is a small central peak. We define two different crater radii: R_0, the radius of the crater at $z=0$, and R_r, the radius at the highest point on the crater rim. R_0 is generally larger than R_{fit}, the equivalent radius obtained from the hyperbolic fit, as the fit and the real profile start to diverge near $z=0$. R_0 is in fact quite difficult to measure without a digitized profile, but is of particular interest as it marks the boundary between the region of excavation and the region of deposition. The rim radius R_r, on the other hand, is relatively easily measured without a digitized profile, but has no counterpart in the hyperbolic fits. Finally, we define the rim height H_r as the distance from $z=0$ to the highest point on the crater rim.

As with the radius and depth determined from the hyperbolic fits, we find that these dimensions are dependent on the impact energy E, projectile radius r_p, and projectile density ρ_p. In each case, we fit the quantity of interest to a function of the form $AE^{\alpha}r_p^{\beta}\rho_p^{\gamma}$, with coefficient A and the power-law exponents α, β, and γ used as fitting parameters. If a fit involving all three independent variables gave one exponent that was zero within the statistical uncertainties, then that parameter was set to zero and the fit performed using the remaining parameters. As above, uncertainties in the fit parameters were determined using Monte Carlo methods [22].

The results are summarized in Table II. We find that both the fit depth H_{fit}, and the true crater depth H are dependent on impact energy and projectile density, but are independent of projectile size. The crater radius, on the other hand, scales differently depending on where it is measured. The crater radius extracted from the hyperbolic fit, R_{fit}, is dependent on

TABLE II. Impact parameter dependence of crater dimensions. Fitting is to the form $AE^{\alpha}r_p^{\beta}\rho_p^{\gamma}$. In the case that the dependence on a parameter was significantly weaker than the others, this dependence was set to zero and a fit was performed using only the remaining parameters. Results are independent of the size of glass beads comprising the granular target. All uncertainties are estimated using Monte Carlo methods. All quantities are in SI units.

Dimension	A	α	β	γ
Hyperbolic depth, H_{fit}	0.099±0.008	0.210±0.004		−0.264±0.008
Hyperbolic radius, R_{fit}	0.15±0.01	0.226±0.005	0.22±0.02	
Profile depth, H	0.13±0.01	0.197±0.004		−0.309±0.009
Profile radius at $z=0$, R_0	0.143±0.006	0.255±0.003		−0.120±0.005
Radius at rim, R_r	0.28±0.02	0.196±0.004	0.213±0.009	−0.074±0.005
Rim height, H_r	0.16±0.02		1.00±0.03	
Aspect ratio, R_{fit}/H_{fit}	1.5±0.2	0.016±0.006	0.22±0.02	0.264±0.008

impact energy and projectile size, while the true radius at $z=0$, R_0, is also energy dependent but depends on projectile density, not projectile size. The crater radius at the highest point of the rim, R_r, is dependent on impact energy, projectile size, and projectile density. The height of the rim, H_r, is almost perfectly linearly proportional to the projectile radius, and is independent of impact energy and projectile density.

IV. DISCUSSION

We have observed that the interior of simple granular craters are well described by a hyperbolic profile, and that the shape and size of this profile depends systematically on the impact parameters. In discussing the *shape* of the crater profile, we can ignore the crater size and characterize the shape by the aspect ratio, R_{fit}/H_{fit}, and the slope c_{fit}. As we see in Fig. 6, the slope is a function of aspect ratio only, and the profiles therefore belong to a one-parameter family of hyperbolas. The aspect ratio itself is virtually independent of projectile impact energy, but is dependent on the projectile size and density. Craters with different aspect ratios are not merely stretched versions of one another. At small aspect ratios craters are close to conical with a slope that is large compared with other craters, but still well below the angle of repose. As the crater aspect ratio becomes larger, the slope approaches a constant value, around 18°. While the gross morphological transitions from simple to complex craters are found to be highly dependent on impact energy [6], we find that the shape of the simple crater interior is independent of energy, and instead highly dependent on the properties of the projectile used in its formation.

In this work we do not consider the presence or absence of small central peaks, but our results are consistent with those of [6]. Fits were applied to the region just beyond the central peak, if present, and the shape of the crater interior is independent of the presence or absence of a central peak.

We are able to measure the final crater shape only, so we cannot investigate the process by which the crater forms, but we can make some inferences. Upon impact, the projectile forms a transient crater, both by throwing material upwards and pushing it downward and outward. This transient crater is unstable, and collapses under gravity. As with large scale craters [21], the collapse process will shape the final crater profile. If excavation is complete by the time the transient crater collapses, the transient and final craters should have nearly the same volume, but will not have the same shape.

That all the crater profiles belong to a single family of hyperbolas suggests that the collapse process is most likely similar for all craters studied. That the observed crater slopes are consistently smaller than the granular angle of repose may suggest that the collapse process is more complex than simple surface-flow avalanching. That being said, it has been theorized [23] and observed in a cratering context [7] that an unstable granular step will collapse into a step with a slope below the repose angle, where steeper initial steps result in shallower final slopes. This is the result of a thin flow at the granular surface. Our geometry is significantly more complex than that studied in these papers, but this may provide a connection between the transient and final crater shapes. It may also be the case that this shallow angle is a result of the deep fluidization of the granular bed in the vicinity of the transient crater. The fluidized material would evolve toward a flat surface (as a low potential energy state), but the dissipation of energy would cause it to "freeze" before this state is reached [24].

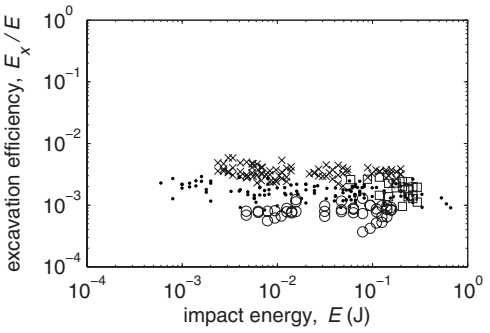

FIG. 7. The ratio E_x/E plotted as a function of the kinetic energy E of the projectile at impact. As in Fig. 4, the different symbols indicate different projectile densities.

Apart from the rim height, which we find to be dependent on projectile size only, our crater dimensions show a strong dependence on impact energy. Crater depths and radii dependent on impact energy only were reported in Ref. [6], but these experiments were performed using only a single projectile. If we limit our fits to a single projectile only, our results are consistent. A variety of projectiles were used in Ref. [12], but in those experiments craters were formed by projectiles which only partially penetrate the surface. This requires a modified definition of both crater radius and depth.

In both Refs. [6,12], the authors report that crater radius scales as $E^{1/4}$. This is the result predicted if most or all of the impact energy is used simply to lift out of the crater volume against gravity and deposit it on the surface [17]. If the crater's radius R and depth are proportional to one another (i.e., if the aspect ratio is constant), then the energy required to excavate the crater will be proportional to R^4, and so $R \propto E^{1/4}$. This is very nearly the energy dependence we find for R_0, while our other measures of crater radius show a slightly weaker energy dependence. Our crater aspect ratio is nearly independent of impact energy, consistent with the assumptions of this argument. We can use our digitized crater profiles to estimate the excavation energy and test the other assumption, namely, that the excavation energy is roughly the same as the impact energy. We define the excavation energy E_x as the energy required to lift the granular material that would have occupied the crater interior to the $z=0$ surface.

$$E_x = \pi \rho_b g \int_0^{R_0} z(r)^2 r \, dr. \tag{3}$$

Here ρ_b is the bulk density of the granular material, assumed to be unchanged by the excavation process, and $z(r)$ is the azimuthally averaged crater profile. The integral is performed in the region of the crater for which $r<R_0$. The results of this analysis are illustrated in Fig. 7, which shows the ratio E_x/E plotted as a function of impact energy.

We find that E_x/E is constant for a given projectile density over three and a half orders of magnitude in impact energy. However, our results show that the excavation energy is only a very small fraction of the total energy delivered by the projectile. E_x/E ranges from less than 0.1% for the high-density tungsten carbide projectiles to about 0.5% for the relatively low-density glass projectiles. This is in clear contradiction with the assumption made in the scaling argument above that most of the impact energy is used to excavate the crater against gravity.

There are at least two reasons why this assumption is not satisfied for our granular craters, while it is believed to apply to large planetary craters [17]. First, the grains are not simply removed from the crater with zero velocity—they are ejected with considerable kinetic energy. Much of this energy is dissipated by collisions and air resistance, making an accurate determination difficult, but by analyzing high-speed video images of the impact process, we estimate that the kinetic energy of the excavated beads is a few times larger than E_x. Second, only a fraction of the projectile's energy is delivered to the target near the surface. The projectile can penetrate quite deeply into the target material [5,10,12,14,15]; energy delivered more than a few projectile radii below the surface will be rapidly dissipated in the interior of the target by friction and interparticle collisions and will not contribute significantly to the cratering process. Recently, Katsuragi and Durian [10] and Royer *et al.* [15] have studied the motion of a projectile as it penetrates a granular target. In both studies, the projectile loses roughly 20% of its energy within one projectile radius of the surface. This is in contrast to what happens in a hypervelocity impact, for which virtually all of the energy is released close to the target surface at the moment of contact as if in an explosion [17].

V. CONCLUSION

In conclusion, we have used laser profilometry to digitize the surfaces of low-energy impact craters, allowing detailed investigation of the crater shape. We find that the interior of the craters are hyperbolic in profile. Crater radius is dependent not only on the impact energy, but also on the projectile size, while the crater depth is dependent on impact energy and projectile density. Crater profiles belong to a family of hyperbolic curves, with a shape dependent on the crater radius to depth aspect ratio. At small aspect ratios craters are more conical than at large aspect ratios, for which the crater slope approaches a constant value. In all cases, the crater slope is well below the angle of repose. Other crater dimensions are also dependent on projectile density and size. We have also shown that the ratio of the energy required to excavate the crater against gravity to the projectile's impact energy is small, due to the fact that only a small fraction of the projectile's energy is delivered near the target surface.

[1] P. H. Schultz, Int. J. Impact Eng. **5**, 569 (1987).
[2] G. S. Collins, H. J. Melosh, J. V. Morgan, and M. R. Warner, Icarus **157**, 24 (2002).
[3] G. S. Collins, H. J. Melosh, and B. A. Ivanov, Meteorit. Planet. Sci. **39**, 217 (2004).
[4] M. A. Cook and K. S. Mortensen, J. Appl. Phys. **38**, 5125 (1967).
[5] J. R. de Bruyn and A. M. Walsh, Can. J. Phys. **82**, 439 (2004).
[6] A. M. Walsh, K. E. Holloway, P. Habdas, and J. R. de Bruyn, Phys. Rev. Lett. **91**, 104301 (2003).
[7] J. F. Boudet, Y. Amarouchene, and H. Kellay, Phys. Rev. Lett. **96**, 158001 (2006).
[8] K. A. Newhall and D. J. Durian, Phys. Rev. E **68**, 060301(R) (2003).
[9] Z. J. Zheng, Z. T. Wang, and Z. G. Qiu, Eur. Phys. J. E **13**, 321 (2004).
[10] H. Katsuragi and D. Durian, Nat. Phys. **3**, 420 (2007).
[11] K. Wada, H. Senshu, and T. Matsui, Icarus **180**, 528 (2006).
[12] J. S. Uehara, M. A. Ambroso, R. P. Ojha, and D. J. Durian, Phys. Rev. Lett. **90**, 194301 (2003).
[13] M. P. Ciamarra, A. H. Lara, A. T. Lee, D. I. Goldman, I. Vishik, and H. L. Swinney, Phys. Rev. Lett. **92**, 194301 (2004).
[14] M. A. Ambroso, C. R. Santore, A. R. Abate, and D. J. Durian, Phys. Rev. E **71**, 051305 (2005).
[15] J. R. Royer, E. I. Corwin, P. J. Eng, and H. M. Jaeger, Phys. Rev. Lett. **99**, 038003 (2007).
[16] H. M. Jaeger, S. R. Nagel, and R. P. Behringer, Rev. Mod. Phys. **68**, 1259 (1996).
[17] H. J. Melosh, *Impact Cratering: A Geologic Process* (Oxford University Press, New York, 1989).
[18] S. Thoroddsen and A. Shen, Phys. Fluids **13**, 4 (2001).
[19] D. Lohse, R. Bergmann, R. Mikkelsen, C. Zeilstra, D. van der Meer, M. Versluis, K. van der Weele, M. van der Hoef, and H. Kuipers, Phys. Rev. Lett. **93**, 198003 (2004).
[20] Ballotini Impact Beads, manufactured by Potters Industries Inc. In order of increasing size, we used Potters Specs *AD*, *AB*, and *C* for our experiments.
[21] H. J. Melosh and B. A. Ivanov, Annu. Rev. Earth Planet Sci. **27**, 385 (1999).
[22] W. H. Press, B. P. Flannery, S. A. Teukolsky, and W. T. Vetterling, *Numerical Recipes in C* (Cambridge University Press, Cambridge, England, 1989).
[23] T. Boutreux and P.-G. de Gennes, Acad. Sci., Paris, C. R. **324**, 85 (1997).
[24] J.-P. Bouchaud, M. E. Cates, J. R. Prakash, and S. F. Edwards, Phys. Rev. Lett. **74**, 1982 (1995).